

Improving Runoff Simulation in the Western United States with Noah-MP and VIC

Lu Su^{a,b}, Dennis P. Lettenmaier^b, Ming Pan^a, Benjamin Bass^c

^a Center for Western Weather and Water Extremes, Scripps Institution of Oceanography,
University of California, San Diego, United States

^b Department of Geography, University of California, Los Angeles, United States

^c Department of Atmospheric and Oceanic Sciences, University of California, Los Angeles,
United States

Correspondence: Dennis P. Lettenmaier (dlettenm@ucla.edu)

Abstract

Streamflow ~~forecasts~~ predictions are critical for managing water resources and for environmental conservation, especially in the water-short Western U.S. Land Surface Models (LSMs), such as the Variable Infiltration Capacity (VIC) model and the Noah-Multiparameterization (Noah-MP) play an essential role in providing comprehensive runoff ~~forecasts~~ predictions across the region. Virtually all LSMs require parameter estimation (calibration) to optimize their predictive capabilities. Here, we focus on the calibration of VIC and Noah-MP models at a $1/16^\circ$ latitude-longitude resolution across the Western U.S. We first performed global optimal calibration of parameters for both models for 263 river basins in the region. We find that the calibration significantly improves the models' performance, with the median daily streamflow Kling-Gupta Efficiency (KGE) increasing from 0.37 to 0.70 for VIC, and from 0.22 to 0.54 for Noah-MP. In general, post-calibration model performance is for watersheds with relatively high precipitation and runoff ratios, and at lower elevations. At a second stage, we regionalized the river basin calibrations using the donor-basin method, which establishes transfer relationships for

Style Definition: Heading 1: Indent: Left: 0.63 cm, Space Before: 0 pt, After: 0 pt, No bullets or numbering, No widow/orphan control

Style Definition: Heading 2

Style Definition: Title

Formatted: French (France)

26 hydrologically similar basins, [via which we extended](#) our calibration parameters to
27 4,816 HUC-10 basins across the [region](#). [Using the regionalized parameters, we show](#)
28 [that the](#) models' capabilities to simulate high and low flow conditions [were](#)
29 substantially [improved](#) following calibration and regionalization. The refined
30 parameter sets [we](#) developed are [intended to support](#) regional hydrological studies and
31 hydrological [assessments of](#) climate change [impacts](#).

32

33 **[1. Introduction](#)**

34 Streamflow [forecasts-predictions](#) play a key role in [various aspects of](#) water and
35 environmental management, especially in the [water-stressed](#) Western U.S. (WUS). In
36 the short term, these [forecasts-predictions](#) provide early warnings for impending flood
37 events, thereby enabling timely preparation and response to mitigate immediate flood
38 risk and damages (Maidment, 2017). They also serve as crucial input for managing
39 reservoirs effectively for water supply (Raff et al., 2013), hydroelectric power
40 generation (Boucher & Ramos, 2018), and river navigation (by providing a basis for
41 predicting water levels) (Federal Institute of Hydrology, 2020). In the longer term,
42 streamflow [forecasts-predictions](#) enable water utilities and agencies to plan water
43 distribution within and across multiple uses—urban, agricultural, and industrial—
44 which is especially vital during drought conditions when efficient water use becomes
45 a necessity (Anghileri et al., 2016;). Streamflow [forecasts-predictions](#) also aid in
46 understanding and [predicting-foreseeing](#) the impacts of climate change on water
47 systems, thereby informing adaptive strategies for water resource management. Thus,
48 in both short and longer-term contexts, streamflow [forecasts-predictions](#) are an
49 important tool for promoting sustainable water practices and resilience to water-
50 related challenges.

51 Streamflow [forecasts-predictions](#) are derived via a synthesis of

52 hydrometeorological data, statistical methodologies, and computational modeling.
53 Direct measurement of runoff is an important element of [streamflow forecasts](#)
54 [process](#), however it is only possible in river basins with well-developed observational
55 infrastructure (Sharma and Machiwal, 2021). This limitation leaves vast areas, often
56 critical to water resource management and climatology, without direct runoff
57 observations on which to base streamflow [forecasts](#)[predictions](#). As an alternative,
58 Land Surface Models (LSMs) can be used to simulate streamflow. LSMs typically are
59 forced with air temperature, precipitation and other [surface](#) meteorological
60 [forcings](#)[variables](#). By integrating climatic, topographic, and land-use information,
61 they can fill streamflow observation gaps and provide comprehensive, spatially
62 distributed runoff [forecasts](#)[predictions](#) (Fisher and Koven, 2020). The capabilities of
63 LSMs equip us with the necessary tools to produce streamflow [forecasts](#)[predictions](#)
64 that can be used to prepare for severe weather conditions, form the basis for water
65 resource management, and inform water management associated with our evolving
66 climate. These benefits hold true irrespective of the limitations associated with direct
67 streamflow observations. Through off-line simulations and reconstructions, LSMs
68 enable us to gain insights into land surface hydrology at various scales - regional,
69 continental, and global.

70 [The p](#)Parameterizations of the underlying hydrological processes [varies](#)[vary](#)
71 across different LSMs, but virtually all models require some level of parameter
72 estimation based on historical observed streamflow data at forecast point, to ensure
73 trustworthy predictions throughout the region (Beven, 1989; Troy et al., 2008; Gong et
74 al., 2015). In cases where observations don't exist, parameters can be transferred from
75 river basins where they do (Arsenault and Brissette, 2014). In cases where
76 observations do exist but aren't current, shorter [records of](#) historical streamflow data
77 [can be used](#) for model calibration and subsequently streamflow [forecasts](#)[predictions](#)

78 can be produced using meteorological forcings for more recent periods when
79 streamflow data aren't available.

80 Implementation of hydrological models for the above purposes usually involves
81 calibration of model parameters using streamflow observations, which are more
82 readily available than other model prognostic variables like soil moisture or
83 evapotranspiration (Demaria et al., 2007; Gao et al., 2018; Troy et al., 2008; Yadav et
84 al., 2007). Calibration has always been a critical and evolving component of
85 hydrologic model application, and has been improved by advances in model
86 parameterization, enhanced spatial resolution providing more detailed and accurate
87 spatial information, improved soil/vegetation data, meteorological inputs, and training
88 data. Furthermore, advances in calibration methods and computing power have
89 facilitated regional approaches to model calibration, and inclusion of multiple
90 hydrologic models. Previous, studies often mostly focused on a single hydrologic
91 model due to computational constraints (e.g., Mascaro et al. (2023), Sofokleous et al.
92 (2023), and Gou et al. (2020)). However, we incorporate two models to address
93 structural model uncertainty and to ensure broader applicability of the calibration
94 methods we employ.

95 The Variable Infiltration Capacity (VIC, Liang et al. (1994)) model and Noah-
96 Multiparameterization (Noah-MP, Niu et al. (2011)), which we use here, are widely
97 used hydrologic models both in the U.S. and globally, as highlighted by Mendoza et
98 al. (2015) and Tangdamrongsub (2023). Many previous implementations of VIC for
99 the Western United States (WUS) have been based on the Livneh et al. (2013) data
100 set, and its predecessor, Maurer et al. (2002), which performed initial calibrations
101 across the region. In the case of Noah-MP, Bass et al. (2023) performed manual
102 calibration across the region efforts. Neither of these implementations, however, sets
103 employs globally optimized calibration, as we do here.

Formatted: Font: Not Bold, No underline, Font color: Auto

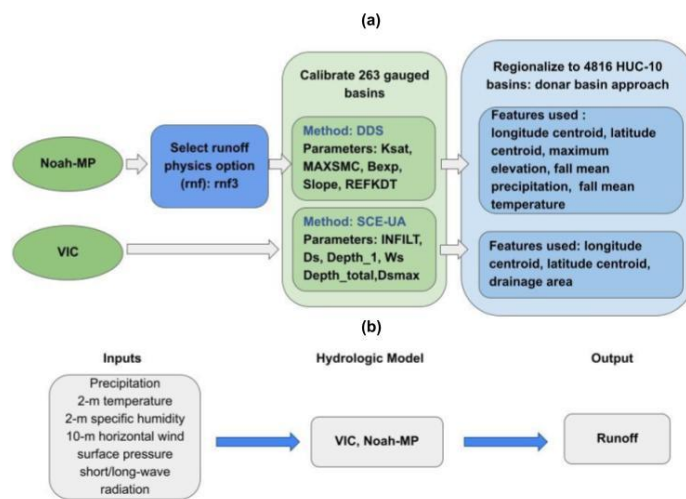
104 The process of calibration can be computationally demanding, and prior research
105 typically has focused on obtaining parameters appropriate to facilitating model
106 simulations that match observations as closely as possible at ~~the observation~~
107 ~~pointstream gauge locations~~ (Duan et al,1992; Tolson and Shoemaker, 2007). Most
108 previous studies have concentrated on a limited number of ~~gauges/river basins~~ ~~basins~~
109 and a single model (e.g. Mascaro et al., (2023); Sofokleous et al., (2023); and Gou et
110 al., (2020)). Here, we aim to establish parameterizations for two LSMs -- ~~the Variable~~
111 ~~Infiltration Capacity (VIC) model~~ and ~~the Noah Multiparameterization (Noah-MP)~~
112 ~~LSM~~ across the ~~entire~~ WUS. ~~Both models have found extensive application both within~~
113 ~~the U.S. and internationally (Mendoza et al.,2015; Tangdamrongsub, 2023).~~ ~~In doing~~
114 ~~so,~~ we apply global optimizationed ~~calibration~~ methods ~~at the river basin level,~~
115 ~~followed by a second stage and~~ regionalization, ~~with the objective of facilitating these~~
116 ~~models to provide reliable runoff simulations.~~

117 ~~Building on the context outlined earlier,~~ ~~o~~The work we report here ~~ur~~ study aims
118 ~~to develop high resolution, optimally calibrationed~~ parameters for the VIC and Noah-
119 ~~MP models that can be implemented at the catchment (Hydrologic Unit Code or HUC)~~
120 ~~10 level across the regionin the WUS.~~ ~~In particular, w~~We explore and elucidate (i) the
121 choice of physical parameterizations and calibration of land surface parameters, (ii)
122 extension of these calibrated parameters to areas without gauges, and (iii) factors that
123 influence calibration efficiency and LSM performance using regional parameter
124 estimates. ~~Following this introduction, Section 2 describes our calibration basins, the~~
125 ~~hydrologic models used, and the forcing dataset. The framework of our procedures is~~
126 ~~illustrated in Figure 1. Section 3 provides an in-depth exploration of the calibration~~
127 ~~process.~~ In the case of Noah-MP, which offers multiple runoff generation (physics)
128 options, our initial step involves choosing the most effective runoff parameterization
129 option. Following this, we perform the calibration of land surface parameters. In the

130 case of the VIC model, the runoff parameterization scheme is predetermined, so we
 131 commence immediately with calibration [at 263 river basins](#) across [our region](#). Our
 132 [second stage regionalization \(section 4\) extends](#) the calibrated parameters to ungauged
 133 basins [using the](#) technique known as the donor basin method, as implemented by Bass
 134 et al. (2023). [In Section 5,](#) we evaluate both flood and low flow simulation skills [both](#)
 135 [pre- and post-calibration, and following](#) regionalization. [Finally, following discussion](#)
 136 [and interpretation \(section 6\) section 7 presents conclusions, encapsulating the insights](#)
 137 [and implications of our study.](#)

138

Formatted: Justified



139

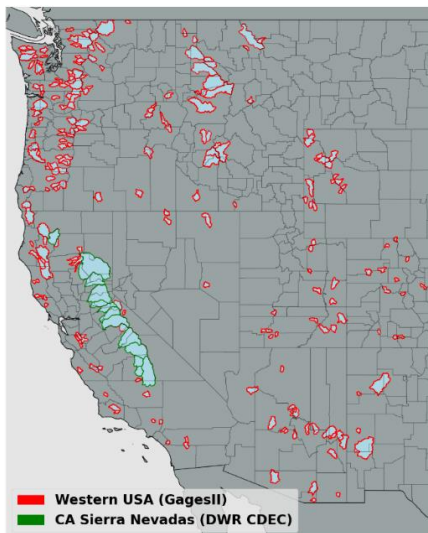
140 [Figure 1 \(a\) framework of the calibration and regionalization processes adopted](#)
 141 [in this study. \(b\) model simulation inputs and output.](#)

142 **2. Study basins, land surface models and forcing dataset overview**

143 **2.1 Study Basins**

144 We selected 263 river basins distributed across the WUS [for calibration of the](#)

145 [two models](#). Most of the basins were from USGS Gages II reference basins (Falcone
146 2011) which have minimum upstream anthropogenic effects such as dams and
147 diversions. Among these basins, our selection criteria included having at least 20
148 years of record, and a minimum drainage area of 144 square kilometers, which is the
149 size of four model grid cells. In addition to 250 Gages II reference stations, we
150 included 13 basins located in California's Sierra Nevada for which [naturalized](#) flows
151 [\(effects of upstream reservoir storage and/or diversions removed\)](#) are available from
152 the California Department of Water Resources (2021). The [locations](#) of the 263 basins
153 [are](#) shown in Figure [24](#). ~~We focused on the hydrological models' calibration to full
154 natural flow (the same as observed streamflow for GAGES II stations; estimated by
155 DWR for the 13 Sierra Nevada sites), which indicates water flow conditions devoid of
156 human interventions like reservoirs or diversions. Each basin was calibrated using We
157 used the most recent 20-year period of streamflow observations for calibration in each
158 of the 263 basins when the observation is available.~~



159
160 Figure. [24](#). 263 river basins for which calibration was performed. The Gages II

161 reference basins are delineated with red boundaries and the CA Sierra Nevadae basins
162 with green boundaries.

163 **2.2 Land Surface Models**

Formatted: Heading 2, Left, Indent: First line: 0 cm

164 The two models we used (VIC and Noah-MP) were chosen due to their broad
165 application and proven effectiveness in hydrological simulations. The VIC model is
166 renowned globally for its success in runoff simulation, as evidenced by studies such as
167 Adam et al. (2003 & 2006), Livneh et al. (2013), and Schaperow et al. (2021).
168 Conversely, Noah-MP, though relatively newer, forms the hydrologic core of the U.S.
169 National Water Model (NWM) and is increasingly used both within the U.S. and abroad.

170 Our selection is further reinforced by a study conducted by Cai et al. (2014), which
171 assessed the hydrologic performance of four LSMs in the United States using the North
172 American Land Data Assimilation System (NLDAS) test bed. This study highlighted
173 Noah-MP's proficiency in soil moisture simulation and its strong performance in Total
174 Water Storage (TWS) simulations, while recognizing VIC's capabilities in streamflow
175 simulations.

176 Our choice of models also was informed by the varying levels of complexity these
177 two models offer in conceptualizing the effects of vegetation, soil, and seasonal
178 snowpack on the land surface energy and water balances (refer to Table 1 for more
179 details). VIC and Noah-MP employ different parameterizations for various
180 hydrological processes, such as canopy water storage, base flow, and runoff. Noah-MP
181 features four runoff physics options (see Table 1). It utilizes four soil layers, each with
182 a fixed depth. In contrast, the VIC model, with its variable infiltration capacity approach
183 (Liang et al., 1994), uses up to three soil layers per grid cell with variable depths,
184 providing flexibility in modeling soil moisture dynamics. The unique runoff generation
185 methodologies of each model are particularly pertinent for capturing the diverse

186 hydrological characteristics of the WUS.
187 The calibrated parameters we develop here for both models will provide future
188 researchers with essential tools for comprehensive hydrological analysis across the
189 WUS. Utilizing these two distinct models, each with unique strengths and methods, will
190 facilitate thorough exploration of the WUS's varied hydrological characteristics, and
191 response of the watersheds in the region to climate change, as well as implementation
192 of improved streamflow forecast methods. Our results will help to facilitates a deeper
193 understanding of hydrological processes and spatial variability across the entire WUS
194 region.

195 In our implementation of both models, we accumulated runoff over each of the
196 calibration watersheds. We chose not to implement the channel routing schemes of
197 either model since their impact on daily streamflow simulations was-is small given
198 the relatively small size of most of the basins. This aligns with earlier research (e.g.,
199 Li et al. 2019). However, in both the case of VIC and Noah-MP, the output of our
200 simulations (runoff) could be used as input to routing models, such as those that are
201 options in the implementation of both models. We describe below the particulars of
202 the two models.

203 **2.2.1 VIC**

204 VIC is a macroscale, semi-distributed hydrologic model (described in detail by
205 Liang et al 1994) that determines land surface moisture and energy states and fluxes by
206 solving the surface water and energy balances. VIC is a research model and in its
207 various forms it has been employed to study many major river basins worldwide (e.g.
208 Adam et al 2003 & 2006; Livneh et al 2013; Schaperow et al 2021). This model enjoys
209 a broad user community — as per the citation index Web of Science, the initial VIC
210 paper has been referenced more than 2600 times, with contributing authors spanning at

Formatted: Justified, First line: 2 ch

211 least 56 different countries (Schaperow et al 2021). We obtained initial VIC model
212 parameters from Livneh et al 2013, who validated model discharges over major
213 CONUS river basins. The origins of the soil and land cover data are outlined in Table
214 1. The version of the VIC model implemented here is 4.1.2, and it operates in energy
215 balance mode. We selected VIC 4.1.2 for two key reasons: First, our initial parameters
216 were based on Livneh et al. (2013), who validated model discharges over major
217 CONUS river basins using this model version. Second, in a preliminary assessment of
218 snow water equivalent (SWE) simulation skills at select SNOTEL sites across the WUS,
219 we found that VIC 4.1.2 demonstrated superior performance compared to VIC 5 (see
220 Figure S1). This finding, coupled with our research group's extensive experience and
221 proven results with VIC 4.1.2, informed our decision to use this version.

Commented [DL1]: You need to show some of those results in the supplement.

222 2.2.2 Noah-MP

223 Noah-MP was originally designed as the land surface scheme for numerical
224 weather prediction (NWP) models like the Weather Research and Forecasting (WRF)
225 regional atmospheric model. Currently, it's being utilized for physically based,
226 spatially-distributed hydrological simulations as a component of the National Water
227 Model (NWM) (NOAA, 2016). It enhances the functionalities of the Noah LSM (as per
228 Chen et al., 1996 and Chen and Dudhia, 2001) previously used in NOAA's suite of
229 numerical weather prediction models by offering multiple options for key processes
230 that control land-atmosphere transfers of moisture and energy. These include surface
231 water infiltration, runoff, evapotranspiration, groundwater movement, and channel
232 routing (see Niu et al., 2007; 2011). The model has been widely used for forecasting
233 seasonal climate, weather, droughts, and floods not only across the continental United
234 States (CONUS) but also globally (Zheng et al., 2019). We utilized the most current
235 version (WRF-HYDRO 5.2.0)

Formatted: Justified

236 2.3 Forcing Dataset

237 We ran both models at a 3-hour time step and at $1/16^\circ$ latitude–longitude spatial
238 resolution. The forcings were the gridded observation dataset developed by Livneh et
239 al (2013) and extended to 2018 by Su et al (2021) (hereafter referred to as L13). This
240 data set spans the period from 1915 to 2018. For the VIC model, the L13 dataset
241 provided daily values of precipitation, maximum and minimum temperatures, and
242 wind speed (additional variables used by VIC including downward solar and
243 longwave radiation, and specific humidity, are computed internally using MTCLIM
244 algorithms as described by Bohn et al. (2013)). The Noah-MP model, on the other
245 hand, necessitated additional meteorological data such as specific humidity, surface
246 pressure, and downward solar and longwave radiation, in addition to precipitation,
247 wind speed, and air temperature. We used the MTCLIM algorithms, as detailed by
248 Bohn et al. (2013), to calculate specific humidity and downward solar radiation. We
249 employed the Prata (1996) algorithm to compute the downward longwave radiation.
250 Additionally, we deduced surface air pressure by considering the grid cell elevation in
251 conjunction with standard global pressure lapse rates. Following this, we transitioned
252 the daily data to hourly metrics using a cubic spline to interpolate between Tmax and
253 Tmin, and derived other variables using the methods explained by Bohn et al. (2013).
254 Lastly, we distributed the daily precipitation evenly across three hourly intervals.

255 We used a 3-hour simulation timestep given numerical considerations with
256 Noah-MP (which don't affect VIC, however for consistency we used a 3-hour
257 timestep for VIC as well. Despite the fact that precipitation in particular was available
258 daily (and hence apportioned equally to 3-hour timesteps) resolving the diurnal cycle
259 is sometimes important in the case of snow (accumulation and ablation) processes
260 which vary diurnally.

Table 1. Overview of hydrologic model components and parameter data sources.

MODEL	SNOW ACCUMULATION AND MELT	MOISTURE IN THE SOIL AND COLUMN/SURFACE RUNOFF	BASE FLOW	CANOPY STORAGE	VEGETATION DATA	SOIL DATA
VIC (V4.1.2)	Two-layer energy-mass balance model	Infiltration capacity function. Vertical movement of moisture through soil follows 1D Richards equation. (1) TOPMO DEL-based runoff scheme (2) Simple TOPMO DEL-based runoff scheme with an equilibrium water table (hereafter SIMTOP)	A function of the soil moisture in the third layer. Linear below a soil moisture threshold and becomes nonlinear above that threshold. [Liang et al., 1994] Simple groundwater (hereafter SIMGM) [Niu et al., 2007]. Similar to SIMGM, but with a sealed bottom of the soil column [Niu et al., 2005]	Mosaic representation of different vegetation coverages at each cell.	University of Maryland 1-km Global Land Cover Classification (Hansen et al. 2000)	1-km STATSGO database (Miller and White 1998).
NOAH-MP (WRF-HYDRO 5.2.0)	Three-layer energy-mass balance model that represents percolation, retention, and refreezing of meltwater within the snowpack.	(3) Infiltration-excess-based surface runoff scheme [Schaake et al., 1996] (4) BATS runoff scheme, which parameterized surface runoff as a 4th power function	Gravitational free-drainage subsurface runoff scheme [Dickinson et al., 1993]	Semi-tile approach for computing longwave, latent heat, sensible heat and ground heat fluxes	MODIS 30-second Modified IGBP 20-category land cover product	1-km STATSGO database (Miller and White 1998).

Formatted Table

Formatted: French (France)

of the top
2 m soil
wetness
(degree
of
saturation)

262 **3. Model calibration**

263 **3.1 Calibration methods**

264 The initial step in our calibration effort was to optimize the land surface parameters
265 of the two models for the 263 WUS basins. These parameters, primarily soil properties
266 which can exhibit a substantial degree of uncertainty, were iteratively updated via
267 hundreds of simulations to accurately reflect streamflow conditions in each basin.

268 Our focus on calibrating soil-related parameters was based on their critical role in
269 runoff generation. In this respect, we focused on key processes including infiltration,
270 soil moisture storage, and groundwater recharge. The calibration of parameters that
271 control these processes was prioritized to improve the representation of soil-water
272 interactions, a major driver of runoff variability in the region. Given the importance of
273 snow processes across much of the region, we conducted snow simulation verification
274 at 20 Snow Telemetry (SNOTEL) (Natural Resources Conservation Service, 2023)
275 sites across WUS. Our assessment (see Figure S1) indicated that the existing
276 parameterizations for snow processes in both models reproduced observed SWE well
277 across our study region.

278 Prior to calibration, we conducted a sensitivity analysis to identify the most
279 influential parameters for streamflow simulation in both models. We also drew
280 on insights from previous research in this respect (Mendoza et al. 2015; Hussein 2020;
281 Shi et al. 2008; Holtzman et al., 2020; Bass et al., 2023; Schaperow et al., 2023). We
282 then performed a sensitivity analysis, focusing on how variations in the most sensitive

283 ~~se~~ parameters impacted Kling-Gupta Efficiency (KGE; Gupta et al., 2009) KGE
284 ~~outeomes~~. Based on these analyses, we chose to calibrate six parameters for the VIC
285 ~~model and five for the Noah-MP model (Table 2)~~. For each parameter, we defined a
286 physically viable range (refer to Table 2), drawing from values utilized in prior studies
287 (Cai et al. 2014; Mendoza et al. 2015; Hussein 2020; Shi et al. 2008; Gochis et al., 2019;
288 Holtzman et al., 2020; Lahmers et al. 2021; Bass et al., 2023; Schaperow et al., 2023).
289 ~~Through our iterative calibration method, each subsequent simulation learns from the~~
290 ~~previous ones using algorithms designed to reduce the discrepancy between the~~
291 ~~simulated and observed streamflow.~~

292 In recent years, the development of hydrologic model calibration has evolved
293 from manual, trial-and-error approaches to advanced automated techniques. This has
294 included a shift towards global optimization methods, notably the Shuffled Complex
295 Evolution algorithm (SCE-UA; Duan et al., 1992). Typically, SCE-UA has been
296 applied to computationally efficient models (simulation time often on the order of a
297 few minutes or less; see e.g., Franchini et al., (1998)). However, its application
298 becomes less practical with more recent distributed hydrologic models such as the
299 Noah-MP which require longer simulation times. To address these computational
300 challenges, Tolson and Shoemaker (2007) introduced the Dynamically Dimensioned
301 Search (DDS) algorithm, tailored for complex, high-dimensional problems. DDS is
302 more computationally efficiency than SCE-UA, and we therefore used it for our
303 Noah-MP calibrations.

304 Our selection of calibration algorithms was guided by the need to balance
305 computational efficiency with robustness. In the calibration of the VIC model, we
306 employed SCE-UA. This method is a global optimization method widely used in
307 hydrology and environmental modeling, owing to its robustness and efficiency when
308 addressing complex, non-linear, and multi-modal objective functions (Nacini et al.,

Formatted: First line: 0 ch

Formatted: Font: (Asian) +Body Asian (新細明體), (Asian)
Chinese (Traditional, Taiwan)

309 ~~2015). The SCE-UA is well established and widely recognized for its efficacy with~~
310 ~~this particular model (and with which we have considerable experience). The SCE-~~
311 ~~UA has been a benchmark in calibrating VIC for decades (see Naeini et al., 2019).~~
312 ~~The computational efficiency of VIC made SCE-UA a suitable choice, despite its~~
313 ~~requirement for a higher number of iterations. In practical terms, iterating a 20-year~~
314 ~~simulation in VIC takes about 2 minutes for a mid-sized basin, which we found~~
315 ~~manageable in terms of the computer resources available to us.~~

316 For VIC parameter estimation, we employed the Shuffled Complex Evolution
317 algorithm developed at the University of Arizona (SCE-UA, Duan et al. 1992). ~~This~~
318 ~~method is a global optimization method widely used in hydrology and environmental~~
319 ~~modeling, owing to its robustness and efficiency when addressing complex, non-~~
320 ~~linear, and multi-modal objective functions (Naeini et al., 2015).~~

321 For the Noah-MP model, which requires more computational core hours per
322 simulation, we used the ~~DDS method~~. NOAA employs the DDS algorithm for their
323 CONUS implementation of NWM, which is grounded in Noah-MP (Gochis et al. 2019).
324 ~~Although we had not used DDS previously, the fact that we had available to us a~~
325 ~~computational structure which embedded Noah-MP, in addition to its computational~~
326 ~~efficiency, was a deciding factor.~~

327 ~~To assure that the parameter sets we estimated weren't dependent on the~~
328 ~~optimization method, we conducted a comparison between SCE-UA and DDS for~~
329 ~~calibrating VIC across 20 randomly chosen basins. We found that the DDS algorithm~~
330 ~~achieved optimal calibration with fewer iterations (typically around 3000 iterations vs~~
331 ~~only about 250 for DDS). The parameter sets identified were nearly identical, affirming~~
332 ~~our decision to use distinct algorithms tailored to the computational demands of each~~
333 ~~model. We evaluated both calibration methods (DDS and SCE-UA) for VIC for 20~~
334 ~~randomly chosen basins, and obtained similar results. For VIC, we chose SCE-UA due~~

Formatted: Justified

335 ~~to its inherent compatibility with the model and because the additional computation~~
 336 ~~(relative to DDS) was less important given that the inherent computation required for~~
 337 ~~VIC is considerably less than for Noah-MP. While it was possible to calibrate all basins~~
 338 ~~using DDS, the similar outcomes for the chosen basins with both algorithms did not~~
 339 ~~necessitate this approach. (we note that we performed calibration on all of the basins~~
 340 ~~for VIC before starting with the Noah-MP calibration). While using the same calibration~~
 341 ~~method for both models could simplify comparisons, as noted above, the two methods~~
 342 ~~produce essentially the same results, the only difference being computational efficiency.~~

Formatted: Font: (Asian) +Body Asian (新細明體), (Asian) Chinese (Traditional, Taiwan)

343 In our application of SCE-UA, we performed a maximum of 3000 iterations for
 344 each basin, while the DDS method employed 250 iterations for each basin for Noah-
 345 MP. Each basin was calibrated using the most recent 20 years of streamflow data. For
 346 both models, our objective function was the ~~Kling-Gupta Efficiency (KGE, Gupta et~~
 347 ~~al., 2009)~~ metric for daily streamflow. KGE is a widely used performance measure
 348 because of its advantages in orthogonally considering bias, correlation and variability
 349 (Knoben et al., 2019). KGE = 1 indicates perfect agreement between simulations and
 350 observations; KGE values greater than -0.41 indicate that a model improves upon the
 351 mean flow benchmark (Knoben et al., 2019).

352 TABLE 2. Calibration methods, parameters and modifications to their initial
 353 default values evaluated in the calibration.

Model	VIC		Noah-MP	
Calibration Method	SCE-UA		DDS	
Iterations	3000		250	
Calibrated Parameter	Variable Infiltration Curve Parameter (INFILT)	0.001 – 0.4 (Shi et al.,2008)	Saturated Hydraulic Conductivity (Ksat)	2×10^{-9} to 0.07 (Cai et al.,2014)
	Baseflow parameter (Ds)	0.001 – 1.0 (Shi et al.,2008)	Saturation soil moisture content (MAXSMC)	0.1 to 0.71 (Cai et al.,2014)

Formatted Table

Formatted: French (France)

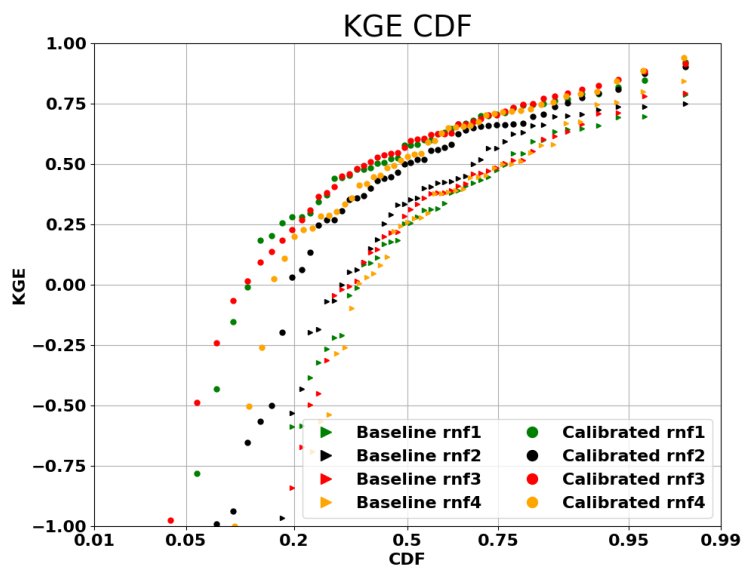
Thickness of Soil in Layer 1 (Depth_1)	0.01 – 0.2 (Shi et al.,2008)	Pore size distribution index (Bexp)	1.12 to 22 (Cai et al.,2014; Gochis et al.,2019)
Total thickness of soil column (Depth_total)	0.6 – 3.5 (Shi et al.,2008)	Linear scaling of “openness” of bottom drainage boundary (Slope)	0.1-1 (Lahmers et al 2021)
Max velocity parameter of baseflow (Dsmax)	0.001 – 30 (Schaperow et al.,2023)	Parameter in surface runoff (REFKDT)	0.1-10 (Lahmers et al 2021)
Fraction of max soil moisture where nonlinear baseflow occurs (Ws)	0.001 – 1 (Shi et al.,2008)		

Formatted: French (France)

354 3.2 Noah-MP parameterization

355 As specified in Table 1, Noah-MP has four runoff and groundwater physics
356 options (rnf). Initially, we adopted the options that are incorporated in the NWM, as
357 elaborated in Gochis et al. (2020). Before we could proceed with calibrating Noah-
358 MP for all the WUS basins, it was necessary to determine suitable rnfs. To streamline
359 computational time, we initially selected 50 basins randomly from the total of 263
360 from which we created four experimental groups. Each group employed a different
361 rnf option. We applied the DDS method to these groups and compared the cumulative
362 distribution functions (CDF) of their baseline and calibrated KGEs (Figure 32). From
363 this figure, it's apparent that the KGE improved post-calibration for all four rnfs.
364 Notably, rnf3, also known as free drainage, exhibited the most substantial

365 performance enhancement after calibration. As a result, we chose to continue using
 366 this option which is incorporated in the NWM. Nonetheless, it's worth noting that the
 367 use of different options for different basins—a feature currently not utilized in Noah-
 368 MP or WRF-Hydro—could potentially result in improved overall model performance.



369
 370 Figure 32. Streamflow performance (KGE of daily streamflow simulations) of
 371 different Noah-MP runoff generation options across 50 (of 263) randomly selected
 372 basins. The performances are shown for both baseline and calibrated simulations.

373 3.3 Calibration of gauged basins

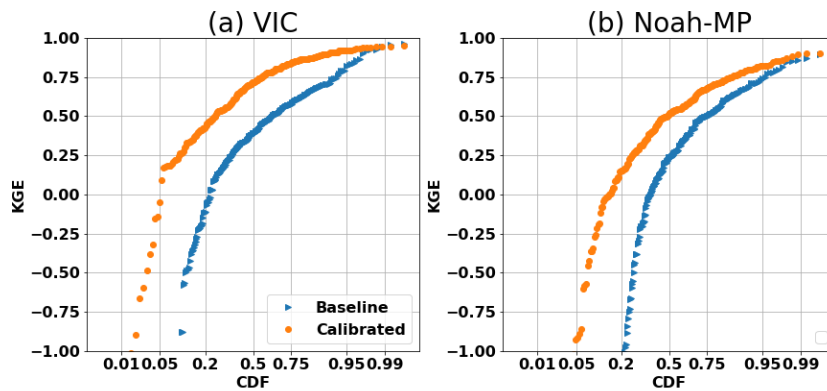
374 Following the selection of the most effective set of runoff generation options
 375 across the domain, we estimated model parameters for all 263 basins. The
 376 comparative performance of the models, before and after calibration, is shown in
 377 Figure 43. It's apparent from the figure that both Noah-MP and VIC have significantly
 378 enhanced their daily streamflow simulation skills post-calibration. After calibration,
 379 the median KGE of Noah-MP improved from 0.22 to 0.54, and the VIC's median

380 KGE increased from 0.37 to 0.70. When contrasting the two models, we observed that
381 VIC outperformed Noah-MP both pre- and post-calibration. One possible explanation
382 could be that the baseline VIC parameters were taken from Livneh et al. (2013), and
383 these parameters had already been validated and adjusted for major U.S. basins
384 (although not for our 263 basins specifically), while the Noah-MP parameters are
385 default values from NWM. Another possibility is inherent differences in the physics
386 of streamflow simulation between the two models (VIC primarily generates runoff via
387 the saturation excess mechanism), although that isn't the main focus of our research.

388 Following the calibration with data from the past 20 years, we performed a test
389 where we calibrated the streamflow using the first 10 years of data and validated with
390 the subsequent 10 years of data. This test revealed that the KGE distribution from the
391 10-year calibration is similar to that from the 20-year data. The median KGE values
392 for VIC and Noah-MP after calibration with 10 years of observations were 0.52 and
393 0.69, respectively. Correspondingly, the median KGEs during the validation period
394 were 0.50 and 0.68, respectively, which are only slightly lower. These comparisons
395 demonstrate general consistency over time in the performance of the calibrated
396 parameters.

397 To validate the robustness of our calibration methodology, we calculated
398 alternative (to KGE) performance metrics, specifically Nash-Sutcliffe Efficiency
399 (NSE) and bias. Our analyses, detailed in Figures S2&3, revealed significant
400 enhancements in model performance as measured by these metrics. The observed
401 improvements across multiple evaluation criteria affirm the efficacy of our calibration
402 process, and in particular that the performance of our procedures is not contingent
403 upon the choice of evaluation metrics.

404



405

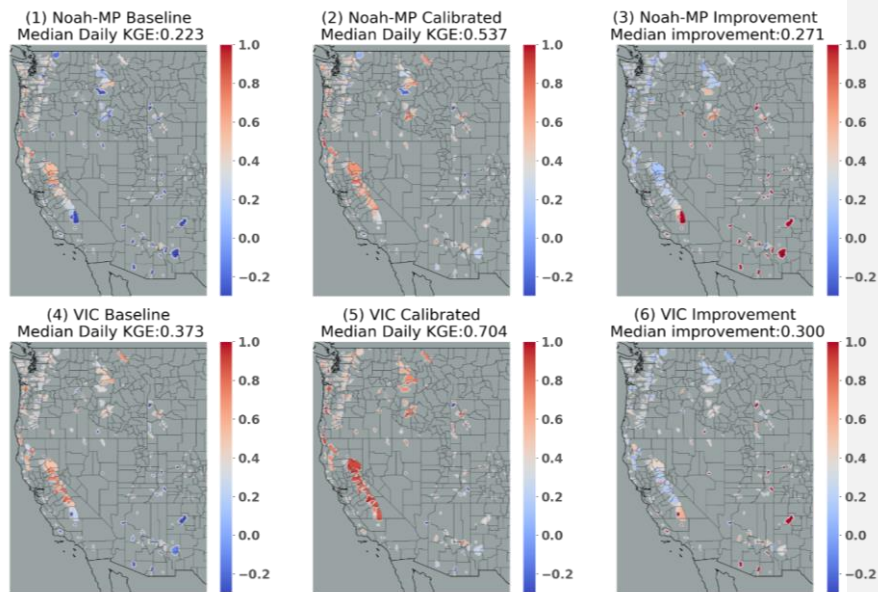
406 Figure 43. Cumulative Distribution Function (CDF) plot of the daily streamflow
 407 KGE for (a) VIC and (b) Noah-MP, comparing baseline and calibrated runs across all
 408 263 basins.

409 We examined the spatial variability of daily streamflow KGE for Noah-MP and
 410 VIC, both before and after the calibration (see Figure 54). The highest baseline KGEs
 411 are along the Pacific Coast, in central to northern CA for both models. VIC's baseline
 412 KGE generally is high in the Pacific Northwest. Post-calibration improvements
 413 occurred for both models in most areas, especially in regions where the baseline KGE
 414 was low, such as southern CA and the southeastern part of the study region. Median
 415 improvements after calibration were 0.27 for Noah-MP and 0.30 for VIC.

416 We observed that basins displaying higher KGE values typically were more
 417 humid than those with lower KGE. To further delve into the relationship between
 418 KGE and basin characteristics, we explored correlations between KGE and 21
 419 different characteristics, including drainage area, elevation, seasonal/annual average
 420 temperature and precipitation, annual maximum precipitation, and seasonal/annual
 421 runoff ratio. Of these, 12 characteristics were statistically significantly correlated with
 422 the VIC KGE, including four seasonal and annual runoff ratios; mean precipitation in
 423 winter, spring, and fall; annual maximum precipitation; and minimum elevation.

424 Figure 65 shows scatterplots of eight representative characteristics. Apart from
425 minimum elevation and mean summer temperature, all other characteristics were
426 positively correlated with KGE. Typically, spring runoff ratio, annual runoff ratio,
427 mean annual max precipitation, and mean winter precipitation exhibited the highest
428 correlations with KGE. This implies that basins with higher runoff ratios (particularly
429 in spring), higher precipitation (especially maximum precipitation), lower summer
430 temperature, and lower elevation are more likely to exhibit strong VIC performance.
431 The same applies to Noah-MP, as indicated in Figure 76, although Noah-MP showed
432 relatively weaker correlations. Correlations between mean summer temperature and
433 mean fall precipitation and Noah-MP KGE weren't statistically significant.

434 The spatial distribution of the eight characteristics is qualitatively similar with
435 the KGE spatial distribution, as shown in Figure 87. Generally, basins with higher
436 KGE have higher characteristic values when the correlation is positive, and lower
437 characteristic values when the correlation is negative. As noted above, both models
438 show good baseline performance along the Pacific Coast, and in central to northern
439 CA (Figure 5). Those areas have high runoff ratios (specifically spring and annual)
440 and high mean winter precipitation. These features generally lead to runoff physics
441 that have infiltration are dominated by the -saturation-excess mechanism, which is
442 well represented by both ~~thus both~~ VIC and Noah-MP. VIC's baseline KGE generally
443 is high in the inland Northwest which has somewhat lower ~~mean annual max daily~~
444 precipitation-runoff ratios and (relatively) deeper groundwater tables. VIC's superior
445 performance relative to Noah-MP may also be because of its variable rather than fixed
446 soil moisture depths (as is the case for Noah-MP).



447

448

Figure 54. Spatial distribution of daily streamflow KGE for Noah-MP baseline

449

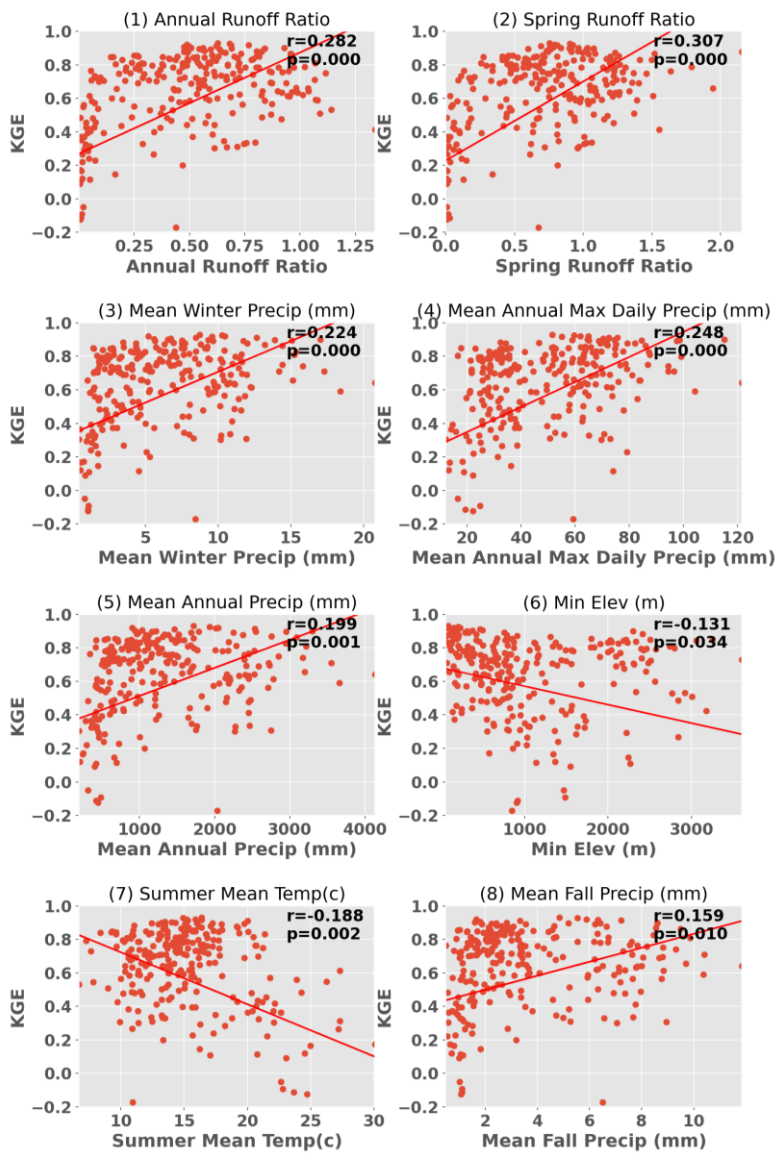
(1); calibrated Noah-MP (2); difference between calibrated and baseline Noah-MP

450

(3); VIC baseline (4); calibrated VIC (5); difference between calibrated and baseline

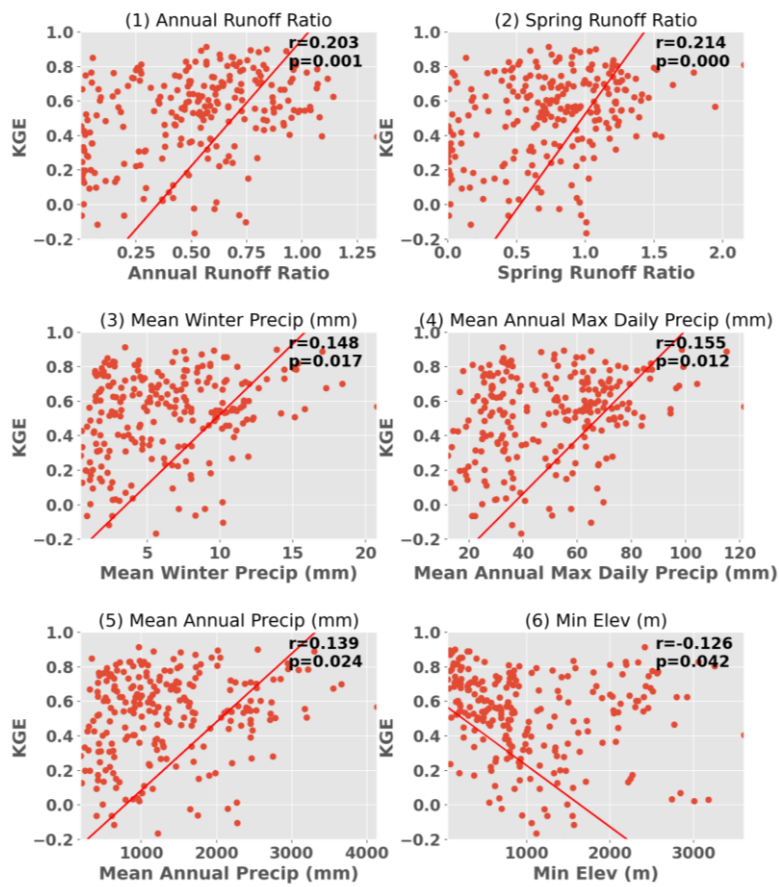
451

VIC (6).



452
 453 Figure 65. Scatterplots of VIC KGE in relation to significantly correlated
 454 characteristics. Each subplot indicates the corresponding Pearson correlation
 455 coefficients and the P-value.

Formatted: Indent: First line: 2 ch



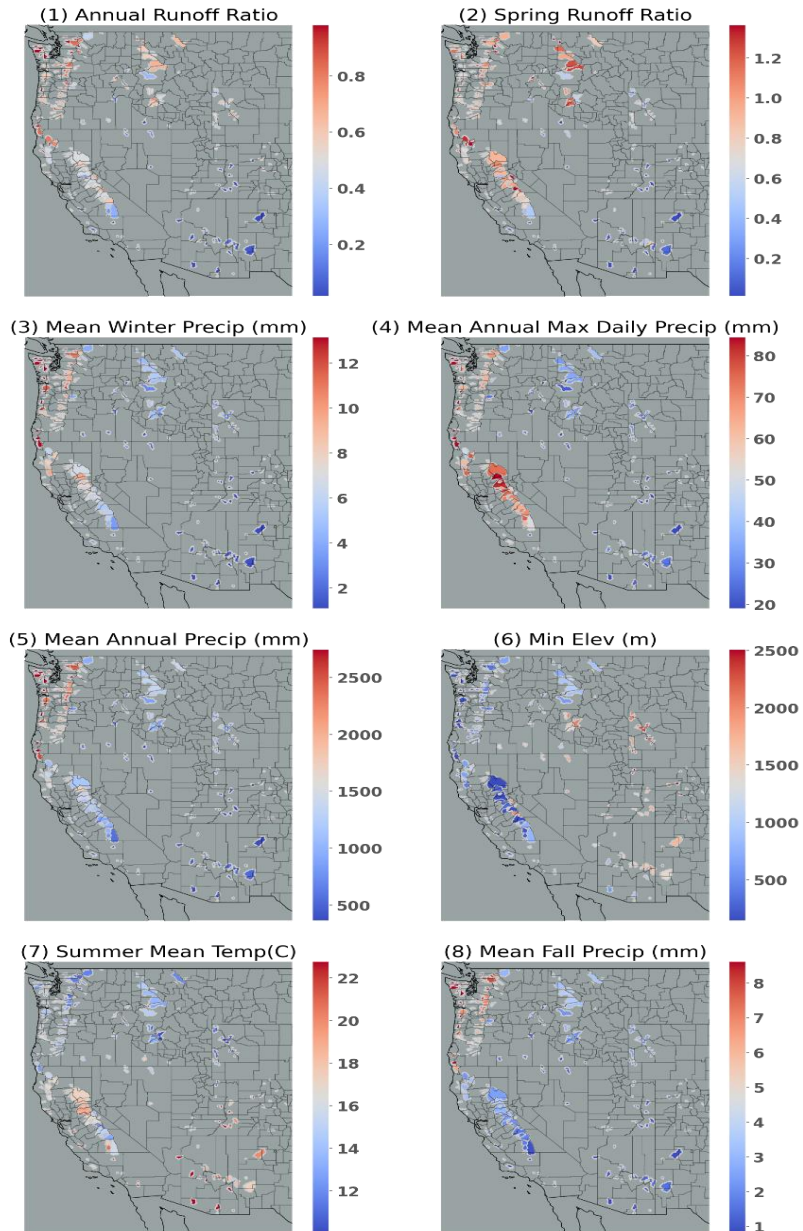
456

457 Figure 76. Scatterplot of Noah-MP KGE in relation to significantly correlated

458 characteristics. Each subplot indicates the corresponding Pearson correlation

459 coefficients and the P-value.

Formatted: Indent: First line: 2 ch



460
 461 Figure 87. Spatial distribution of characteristics that are statistically significantly
 462 correlated with KGE. Note that all characteristics are significantly correlated with
 463 VIC KGE whereas only (1)-(6) are significantly correlated with Noah-MP KGE.

4. Regionalization

To distribute parameters from the calibration basins to the entire region, we used the donor-basin method, where ungauged basins inherit parameters from similar gauged basins. This choice is supported by its successful application in NOAA/NCAR's National Water Model and proven effectiveness in various studies (e.g., as implemented in numerous previous studies (e.g., Arsenault and Brissette (2014); Poissant et al. (2017); Razavi and Coulibaly (2017); Gochis et al. (2019); Qi et al. (2021) and Bass et al. (2023)). The donor-basin approach allows for more accurate and detailed application to ungauged basins, making it a suitable choice for our study.

Following the calibration process, we regionalized the parameters from gauged to ungauged basins based on a mathematical assessment of the spatial and physical proximity between the gauged and ungauged basins, following previous studies by Arsenault and Brissette (2014), and Razavi and Coulibaly (2017). We opted for this method over an alternate approach that first regionalizes the streamflow attributes (such as runoff depth, high flow indicators) and then standardizes the model throughout (as proposed by Castiglioni et al., 2010; Oubeidillah et al., 2014; and Yang et al. 2017). The reason for our choice is our interest in actual streamflow time-series rather than metrics. We carried out the regionalization after calibrating to specific streamflow gauges, ensuring high precision for these gauged basins and facilitating high-quality regionalization in ungauged basins. In hydrology, we considered two primary methods for implementing the donor basin approach. The first uses models calibrated to spatially continuous gridded runoff metrics (Beck et al. 2015; Yang et al. 2019). The second approach, which we ultimately adopted, calibrates models to individual gauges, then extends these parameters to ungauged basins, based either on a statistical or mathematical similarity measures (e.g., Arsenault and Brissette 2014;

Formatted: Indent: First line: 0 ch

490 [Razavi and Coulibaly 2017](#)). Our preference for the second method was guided by a
491 [key limitation of the first approach, specifically it is limited to calibrating against](#)
492 [runoff metrics, such as long-term mean flow and flow percentiles, rather than](#)
493 [streamflow time series. Additionally, their usually coarser resolution compared to](#)
494 [forcing datasets and hydrologic models is a constraint. Our focus on actual](#)
495 [streamflow time series led us to this approach. Specifically, we employed a donor-](#)
496 [basin approach which has demonstrated successful outcomes, as reported by Bass et](#)
497 [al. \(2023\), where an ungauged basin adopts calibrated parameters from its most similar](#)
498 [gauged basin\(s\). This method has been applied in many studies including Arsenault](#)
499 [and Brissette \(2014\); Poissant et al. \(2017\); Razavi and Coulibaly \(2017\); Goehis et](#)
500 [al. 2019; Qi et al. \(2021\); and Bass et al \(2023\).](#)

501 In the donor-basin method, an ungauged basin inherits its land surface
502 parameters from the most similar gauged basin(s) (or the ~~top 'x' 'n'~~ most similar
503 gauged basins). Here, we evaluated the similarity or proximity between gauged and
504 ungauged basins based on the similarity index SI as defined and used by Burn and
505 Boorman (1993) and Poissant et al. (2017):

$$506 \quad SI = \sum_{i=1}^k \frac{|X_i^G - X_i^U|}{\Delta X_i} \quad (1)$$

507 In [Eq. 1](#) ~~this formula~~, k stands for the total number of features considered, X_i^G
508 represents the i th feature of the gauged basin G , X_i^U is the i th feature of a specific
509 ungauged basin, and ΔX_i is the range of potential values for the i th feature, grounded
510 in the data from the gauged basins. This yields a unique value of SI for each gauged
511 basin, contingent on the specific ungauged basin it is compared with. Typically,
512 gauged basins that exhibit greater resemblance to the ungauged basin will have a
513 smaller SI.

514 We assessed the donor-basin method's efficacy using a cross-validation approach,

515 where each gauged basin was treated as ungauged one at a time. The pseudo-
516 ungauged basin inherits its hydrological parameters from its three most similar
517 gauged basins, determined by SI. The parameters inherited are a weighted average
518 from the three donor basins. After testing one to five donor basins, we found that
519 using three donors yielded the best results. Thus, every basin inherits parameters from
520 the three most similar gauged basins in each simulation, offering a concise evaluation
521 of the donor-basin method's regionalization performance.

522 We used 18 basin-specific features in the donor basin method, detailed in Table
523 S1, calculated based on the forcings and parameters used in the study. For feature
524 selection in the donor-basin method, we adopted an iterative approach, explained in
525 detail in the following paragraph. ~~Each iteration added a single feature to the index,~~
526 ~~with the most beneficial feature (based on median KGE improvement) retained. This~~
527 ~~process was repeated until the median KGE no longer improved.~~ Only basins with a
528 KGE exceeding 0.3 were considered, following previous studies suggesting that
529 inclusion of poorly performing basins can lower regionalization performance. We
530 found that a KGE threshold of 0.3 resulted in a median performance improvement of
531 0.08 larger than did a KGE threshold of 0, hence it was chosen. After screening, 223
532 basins were utilized in VIC regionalization and 194 in Noah-MP regionalization. We
533 note that the parameters used for calibration and the features used to determine the
534 similarity index in the regionalization process are different. The physics that control
535 the key hydrological processes of the two models are different, so we explored their
536 best regionalization features separately.

537 To determine the most effective regionalization features from the 18 basin
538 characteristics listed in Table S1, we employed a systematic iterative approach. The
539 first iteration includes 18 simulations, each of which incorporates one of the 18 features.
540 The feature that yielded the greatest increase in the median KGE across all basins, based

Formatted: Left, First line: 0 ch

Formatted: Justified, First line: 2 ch

541 on leave-one-out cross validation, was then retained. In the second iteration, we
542 conducted 17 simulations, each combining the retained feature from the first iteration
543 with one of the remaining 17 features. This process was repeated iteratively, reducing
544 the number of features considered in each subsequent round, until the addition of new
545 features no longer resulted in an appreciable increase in median KGE. The sequence of
546 features shown in Figure 9 (also shown in Table S1) indicated the importance of the
547 features. This iterative approach ensured that each feature's individual and combined
548 contribution to model performance was thoroughly assessed. It allowed us to identify a
549 subset of features that, when used together, optimally improved model accuracy. We
550 recognize the potential existence of inter-feature correlations that may exert a
551 discernible influence on their collective efficacy when utilized in combination.

552 This procedure ~~We resulted in found~~ five features generated the best
553 regionalization performance for VIC (longitude centroid, latitude centroid, maximum
554 elevation, fall mean precipitation, and fall mean temperature). ~~and~~ Three features
555 were found to be best for Noah-MP (latitude centroid, longitude centroid, and
556 drainage area) (see Figure 98). Among them, latitude and longitude are the common
557 features that contribute the most to regionalization when using the similarity index
558 method. This suggests that geographical similarities are the most important factor in
559 parameter information transfer from gauged to ungauged basins.

560 Upon evaluating the performance of baseline, calibrated, and regionalized
561 simulations, the respective median daily KGEs for the VIC model were found to be
562 0.41, 0.71, and 0.49. For the Noah-MP, these values were 0.38, 0.60, and 0.49 (refer
563 to Figures 98 & S49). These metrics are for basins that have a calibrated KGE greater
564 than 0.3 only, resulting in higher median KGEs than for all 263 basins (See Figure
565 43). The KGE distribution also improved overall. It's noteworthy that the
566 regionalization improvement relative to baseline is higher for Noah-MP than for VIC.

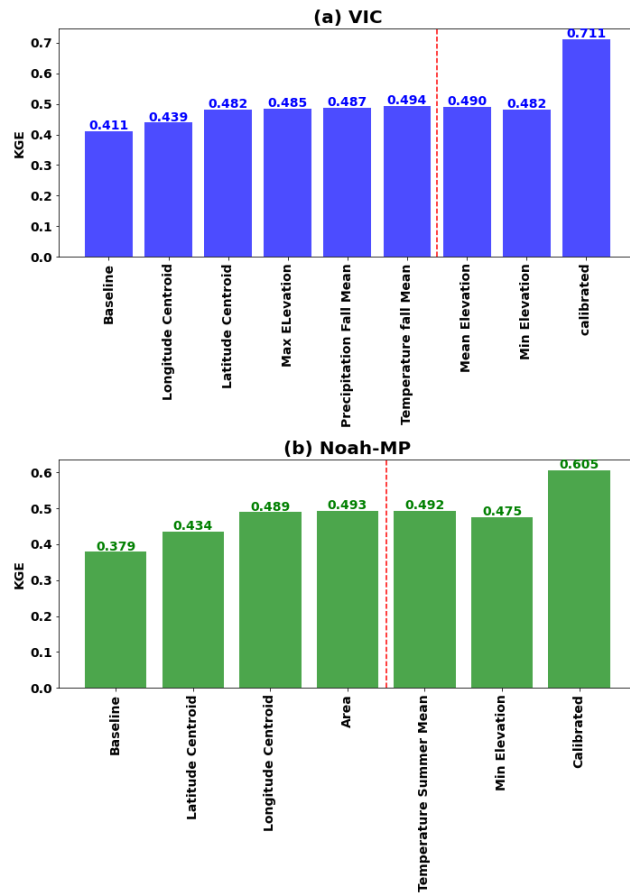
Formatted: Not Highlight

567 While VIC's baseline and calibrated KGE skill distribution outperforms Noah-MP's,
568 the regionalized skills of Noah-MP and VIC are quite comparable. This observation
569 might be attributable to the constraints of the regionalization setup and could warrant
570 future investigation.

571 After optimizing the features and specific design of the donor-basin method,
572 parameters were regionalized to 4816 ungauged USGS Hydrologic Unit Code (HUC)
573 -10 basins across the WUS. HUCs are delineated and quality controlled by USGS
574 using high-resolution DEMs. For each of the 4816 HUC-10 basins, we calculated a
575 similarity index with the calibrated basins using the selected features. The three most
576 similar basins were identified as donor basins, and their weighted average parameters
577 were then adopted by the target HUC-10 basin. The final hydrologic parameters for
578 both VIC and Noah-MP for all WUS HUC-10 basins are shown in Figures S51&S62.
579 The baseline HUC-10 parameters are shown in Figures S73&S84.

580 Comparison of Figures S4-5 to Figures S6-7 makes it clear that the baseline
581 model parameters lack accuracy, and exhibit significant spatial uniformity where large
582 geographical regions share identical parameter values. For example, parameters such
583 as Ds and Soil_Depth1 in VIC show this uniformity. Furthermore, certain parameters,
584 such as SLOPE and REFKDT in the Noah-MP, remained invariant across all spatial
585 domains, and don't reflect real-world conditions. Regionalization, improved the
586 parameters, leading to increased accuracy and strengthening of region-specific
587 characteristics.

Formatted: Indent: First line: 0 ch



590

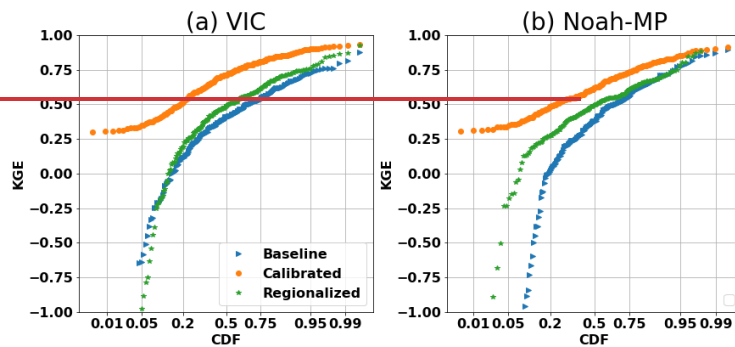
591 Figure 98. Best regionalization features for (a) VIC and (b) Noah-MP. The final

592 regionalization to ungauged basins of the WUS incorporated all features up to the

593 point marked by the red line since the addition of further features doesn't improve

594 KGE.

595



Formatted: Heading 1, Indent: First line: 0 cm

596
597 **Figure 9. CDF of daily KGE for (a) VIC and (b) Noah-MP, comparing**
598 **baseline and calibrated runs across selected regionalized basins within the**
599 **WUS.**

600 5. Evaluation of high and low flow simulation skill

601 Our primary calibration objective was to enhance the accuracy of daily
602 streamflow simulations. However, to ensure the versatility of our parameter sets for
603 research related to both floods and dry conditions, we also evaluate the models'
604 capabilities in reproducing high and low streamflow. To understand the capabilities of
605 the two models in reconstructing high and low streamflow, we assessed their
606 performance across baseline, calibrated, and regionalized settings.

607 (a) Evaluation of high flow performance

608 We used the peaks-over-threshold (POT) method (Lang et al. 1999) to identify
609 extreme streamflow events as in Su et al (2023) and Cao et al. (2019, 2020). We first
610 applied the event independence criteria from USWRC (1982) to daily streamflow data
611 to identify independent events. We set thresholds at each basin that resulted in 3
612 extreme events per year on average. After selecting the flood events over the study
613 period based on the observation, we sorted the floods based on the return period and
614 then calculated the KGE of baseline, calibrated and regionalized floods. Figure [S949](#)
615 displays the associated CDF plots. The median KGE for baseline floods in Noah-MP

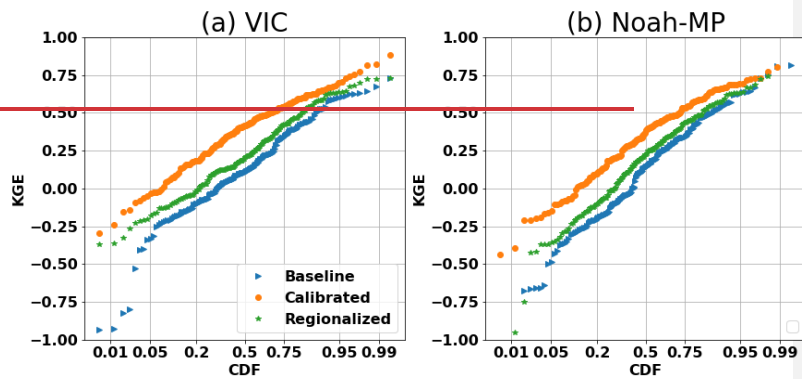
Formatted: Not Highlight

616 was 0.14, which rose to 0.37 post-calibration, and receded to 0.22 after
617 regionalization. For VIC, the flood KGE started at 0.11, increased to 0.41 after
618 calibration, and declined to 0.20 post-regionalization. As anticipated, these numbers
619 are lower than (all) daily streamflow skill due to our calibration target being daily
620 streamflow. Still, flood competencies experienced considerable enhancement,
621 surpassing the Noah-MP KGE benchmark of -0.41 found by Knoben et al. (2019).

622 (b) Evaluation of low flow performance

623 To assess low flow performance, we utilized the 7q10 metric. This hydrological
624 statistic, commonly adopted in water resources management and environmental
625 engineering, is the lowest 7-day average flow that occurs (on average) once every 10
626 years (EPA,2018). Scatterplots of 7q10 (Figure S104) showed high correlation
627 between our model's simulated low flows and the observed data. Post-calibration, this
628 alignment intensified. The VIC model tended to underestimate the low flows. After
629 calibration, the median bias improved from -23.6% to -9.9%, and with
630 regionalization, it was -11.7%. In contrast, Noah-MP began with an 11.20%
631 overestimation in the baseline, improved to 0.61% post-calibration, and was -9.5%
632 after regionalization. The outcomes underline the proficiency of both models for low
633 flow prediction, exhibiting enhanced competencies post-calibration and commendable
634 performance after regionalization.

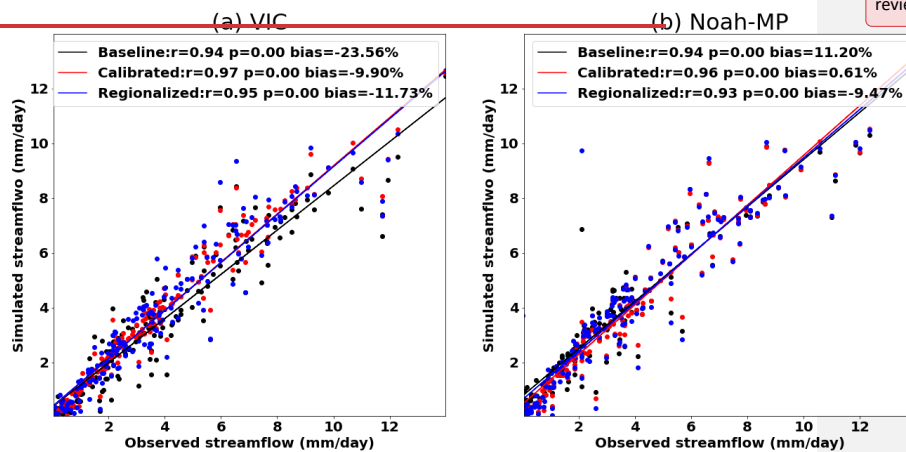
Formatted: Not Highlight



635
636 **Figure 10.** CDF of high flow KGE for (a) VIC and (b) Noah-MP, comparing
637 baseline and calibrated runs across selected regionalized basins within the WUS.

Commented [DL2]: Where are figure 10-11 titles?

Commented [LS3R2]: Moved to supplement as suggested by reviewer



638
639 **Figure 11.** Scatterplot of 7q10 low flows (the lowest 7 day average flow that occurs
640 (on average) once every 10 years) for the baseline and calibrated and regionalized
641 runs for (a) VIC model and (b) Noah-MP. The correlation coefficients, P-values and
642 percentage bias are denoted in the upper section of the figures. The x axis is
643 observed low flow and the y axis is simulated low flow.

644 **6. Discussion**

645 In this discussion, we summarize our key accomplishments in calibrating the two
646 hydrological models, examine our approach to choosing calibration objective

Formatted: Normal, Indent: First line: 0.85 cm

647 functions and metrics, and we consider lessons learned in model regionalization.

648 (a) Improved parameter sets

649 We generated calibrated parameter sets for the VIC and Noah-MP hydrological
650 models at 1/16° latitude-longitude scale across WUS. These calibrated parameter sets
651 are intended to facilitate the use of the two models for climate change and water
652 investigations across the region, among other applications. Our focus on calibrating
653 daily streamflow aligns with common practice in hydrology, providing a
654 comprehensive representation of catchment hydrology dynamics which should enhance
655 future understanding of hydrological phenomena and their spatial variations across the
656 region.

657 (b) Selection of calibration objective function

658 We used objective functions based on streamflow observations. We chose this
659 approach due to its applicability elsewhere, given the widespread accessibility of
660 streamflow observations as compared to alternative metrics such as soil moisture or
661 evapotranspiration (Demaria et al., 2007; Gao et al., 2018; Troy et al., 2008; Yadav et
662 al., 2007). While we acknowledge the potential of remote sensing products like
663 MODIS, SMAP, SMOS, ESA, and ALEXI to improve calibration efforts, especially
664 for variables like actual evapotranspiration (AET) and soil moisture (SM), we were
665 limited by the scarcity of observations for these variables. Future studies could,
666 nonetheless, leverage from the methods we've employed to incorporate additional
667 variables into the objective functions we used.

668 (c) Selection of calibration metric

669 We used the KGE metric applied to daily streamflow, which we chose for its
670 ability to address bias, correlation, and variability simultaneously (Knoben et al.,
671 2019). We also evaluated NSE and BIAS metrics, and found substantial
672 improvements in both models' performance after calibration when these metrics were

Formatted: Font: (Asian) +Body Asian (新細明體)

Formatted: Font: (Default) Times New Roman

Formatted: Font: (Default) Times New Roman

Formatted: Font: (Default) Times New Roman

Formatted: Font: (Default) Times New Roman

Formatted: Font: (Default) Times New Roman

Formatted: Font: (Default) Times New Roman

Formatted: Font: (Default) Times New Roman

Formatted: Font: (Asian) DengXian, (Asian) Chinese (Simplified, Mainland China)

Formatted: Indent: Left: 0.85 cm, First line: 0 ch

Formatted: Font: (Default) Times New Roman

Formatted: Font: (Default) Times New Roman

Formatted: List Paragraph, Numbered + Level: 1 + Numbering Style: a, b, c, ... + Start at: 1 + Alignment: Left + Aligned at: 0.85 cm + Indent at: 1.48 cm

673 used in place of KGE (See Figures S2-3) . Our assessment of high and low flow
674 reconstruction in Section 5 further validated our generated parameter sets. While we
675 used a single objective function due to data and computing constraints, incorporating
676 multiple objective functions is feasible in principle.

677 (d) Regionalization possibilities

678 We calibrated model parameters directly for individual basins, considering their
679 unique hydrological features, and then transferred these calibrated parameters to
680 similar basins based on similarity assessments. Alternative parameter transfer
681 strategies could be used within the same framework we employed (e.g., pedo-transfer
682 functions, e.g. Imhoff et al.,2020) or multiscale parameter regionalization (e.g.
683 Schwepe et al.,2022). We do note that our regionalization approach facilitates the
684 transfer of calibrated parameters to comparable regions, which could be explored in
685 future research.

686 **7. Conclusions**

687 Our intent was to develop a regional parameter estimation strategy for the VIC
688 and Noah-MP land surface schemes, and to apply it across the WUS region at the
689 HUC-10 catchment scale. We've described what we believe is a robust framework
690 that can be applied in future hydrological and climate change studies across the WUS,
691 and is applicable to other regions as well. Our key findings and conclusions are:

692 a) Our catchment scale calibration of the two models to 263 sites across WUS
693 resulted in major improvements in the performance of both models relative to
694 a priori parameters, but performance improvement was greatest for Noah-MP
695 – although this may be in part because VIC a priori parameters benefitted
696 from prior calibration and hence resulted in better baseline performance than
697 did a priori Noah-MP.

698 b) Both models performed best in more humid basins, mainly in the Pacific

Formatted: Normal, Indent: First line: 0.85 cm

Formatted: Font: (Default) Times New Roman

Formatted: Font: (Default) Times New Roman

Formatted: Font: (Default) Times New Roman

Formatted: Font: (Default) Times New Roman

Formatted: Font: (Default) Times New Roman

Formatted: Font: (Default) Times New Roman

Formatted: Font: (Default) Times New Roman

Formatted: Font: (Default) Times New Roman

699 Northwest and central to northern CA where runoff ratios are high. This is
700 consistent with previous results (e.g. Bass et al.,2023).

Formatted: Font: (Default) Times New Roman

701 c) Post-calibration regional model performance improved for both models in
702 most areas, especially where the baseline KGE was low, such as southern CA
703 and the southeastern part of the study region.

Formatted: Font: (Default) Times New Roman

704 d) VIC performance across all calibration basins generally was better than for
705 Noah-MP. However, Noah-MP performance benefitted more from
706 regionalization than did VIC, and ultimately post-regionalization VIC
707 performance was only slightly superior to that of Noah-MP.

708
709 The calibrated parameters, derived from global optimal calibration methods, are
710 set to enhance hydrological simulations and forecasting in the WUS, providing
711 valuable support for regional hydrologic and river hydrodynamic modeling studies.
712 The improved model predictions are expected to benefit water management practices
713 in the region and contribute to a better understanding of climate change impacts.
714 Furthermore, the methodologies employed in this study have broader applicability and
715 can be adapted to other geographic areas, extending the significance of our work
716 beyond the WUS. This research thus contributes to the global effort to improve
717 hydrological system understanding and management.

718 While this study has yielded valuable insights and contributions, we
719 acknowledge certain limitations, including the use of a single objective function and
720 the exclusive focus on streamflow calibration. In future research, we intend to explore
721 additional objective functions and broaden the scope of calibration to include other
722 hydrological variables, thereby further enriching the robustness and applicability of
723 our methodology.

724 Our objective was to produce parameter sets for VIC and Noah MP over WUS

725 that could be used in regional studies, and would result in better model performance
726 than default or other “off the shelf” parameters. We identified preferred runoff
727 generation options for Noah-MP (physics options are fixed in VIC) using a subset of
728 our WUS basins (50 in total) for which we evaluated all four Noah-MP runoff
729 generation options. Once we identified the optimal runoff generation options for
730 Noah-MP, we identified (calibrated) parameters for both Noah-MP and VIC for each
731 of our 263 basins across WUS using the most recently available 20 years of
732 streamflow observations. Following calibration, the Noah-MP median KGE increased
733 from 0.22 to 0.54, while the median VIC KGE rose from 0.37 to 0.70. VIC KGEs
734 were higher than Noah-MP’s both before and after calibration across the 263 basins,
735 possibly because the initial VIC parameters had the benefit of some previous
736 calibration, albeit for much larger river basins across WUS (in the case of post-
737 calibration KGE, it’s unclear whether and how they might have been affected by the
738 choice of initial parameters). Other possible cause of the differences could be
739 inherent differences in streamflow simulation physics between the two models. We
740 also conducted a test using the initial 10 years of data for calibration and the
741 following 10 years for validation, and found results that were consistent with those we
742 obtained using the entire 20 years for calibration.

743 Upon the selection of suitable parameterizations for Noah-MP and calibration of
744 gauged basins for both VIC and Noah-MP, we extended the use of the calibrated
745 parameters to ungauged basins across the WUS for both models. This extension was
746 achieved through the donor-basin regionalization method, which allows ungauged
747 basins to inherit parameters from gauged basins with similar hydroclimatic properties.
748 We discovered that using a weighted combination of three similar basins yielded
749 better regionalization results (in terms of KGE) compared to using the single most
750 similar donor basin, as determined by a similarity index. Following regionalization,

751 the median KGE for VIC rose from 0.41 to 0.49, and for Noah-MP it increased from
752 0.38 to 0.49 over the selected basins. Interestingly, even though the pre-
753 regionalization KGE for VIC was considerably higher than for Noah-MP, the post-
754 regionalization values for the two models were nearly identical. Stated otherwise, the
755 regionalization enhancement was considerably greater for Noah-MP than for VIC.
756 We further evaluated high and low flow simulation skills and found the skill
757 significantly improved after calibration for both VIC and Noah-MP and improvements
758 remained after regionalization. Following calibration and regionalization, we
759 developed gridded parameter sets for both models at 1/16° latitude-longitude
760 resolution for all 4816 HUC-10 basins across the WUS. These parameter sets should
761 be useful for regional hydrologic and river hydrodynamic modeling studies over all or
762 parts of the WUS domain. Improving the accuracy of the models' predictions should
763 have benefits for water management across the region, and more and more generally
764 for understanding the potential impacts of climate change across the region.
765 Moreover, the methods and procedures we utilized are not restricted to our current
766 research domain; they could be transferred readily to other geographic regions. In
767 effect, our research contributes to both local and global efforts to understand and
768 manage our critical hydrological systems better, demonstrating its broader relevance
769 and utility.
770

771 **Data Availability statement**

772 The Livneh (2013) forcings are available at
773 <http://livnehpublicstorage.colorado.edu:81/Livneh.2013.CONUS.Dataset/>. The
774 extended forcings used in this study are available at [ftp://livnehpublicstorage.](ftp://livnehpublicstorage.colorado.edu/public/sulu)
775 [colorado.edu/public/sulu](ftp://livnehpublicstorage.colorado.edu/public/sulu). The results are available online at
776 <https://figshare.com/s/66fe8305bff516e80f6f>.

777

778 **Author contribution**

779 LS and DL conceptualized the study. LS generated the dataset and analysis with
780 support of DL, MP and BB. LS drafted the manuscript with support of DL.

781

782 **Competing interests.** The contact author has declared that none of the authors has
783 any competing interests.

Formatted: Font: (Asian) +Body Asian (新細明體)

784 **References**

- 785 Adam, J.C. and Lettenmaier, D.P.: Adjustment of global gridded precipitation for
786 systematic bias, *J. Geophys. Res.*, 108(D9), 1-14, doi:10.1029/2002JD002499,
787 2003.
- 788 Adam, J.C., Clark, E.A. , Lettenmaier, D.P. and Wood, E.F.: Correction of Global
789 Precipitation Products for Orographic Effects, *J. Clim.*, 19(1), 15-38, doi:
790 10.1175/JCLI3604.1, 2006.
- 791 Anghileri, D., Voisin, N., Castelletti, A., Pianosi, F. , Nijssen, B. and Lettenmaier,
792 D.P.: Value of Long-Term Streamflow Forecasts to Reservoir Operations for
793 Water Supply in Snow-Dominated River Catchments. *Water Resources Research*
794 52: 4209–25, 2016.
- 795 Arsenault, R., and Brissette, F. P.: Continuous streamflow prediction in ungauged
796 basins: The effects of equifinality and parameter set selection on uncertainty in
797 regionalization approaches. *Water Resour. Res.*, 50, 6135–6153, [https://doi.org/](https://doi.org/10.1002/2013WR014898)
798 10.1002/2013WR014898, 2014.
- 799 Bass, B., Rahimi, S., Goldenson, N., Hall, A., Norris, J. and Lebow, Z.J.: Achieving
800 Realistic Runoff in the Western United States with a Land Surface Model Forced
801 by Dynamically Downscaled Meteorology. *Journal of Hydrometeorology*, 24(2),
802 269-283, 2023.
- 803 [Beck, H. E., Roo, A. de and van Dijk, A. I. J. M.: Global maps of streamflow](#)
804 [characteristics based on observations from several thousand catchments. *J.*](#)
805 [*Hydrometeor.*, 16, 1478–1501, <https://doi.org/10.1175/JHM-D-14-0155.1>, 2015.](#)
- 806 Bennett, A. R., Hamman, J. J. and Nijssen, B.: MetSim: A Python package for
807 estimation and disaggregation of meteorological data. *J. Open Source Software*,
808 5, 2042, <https://doi.org/10.21105/joss.02042>, 2020.
- 809 Beven, K.: Changing ideas in hydrology-the case of physically-based models. *Journal*

810 of Hydrology, 105(1-2), 157–172. [https://doi.org/10.1016/0022-1694\(89\)90101-](https://doi.org/10.1016/0022-1694(89)90101-)
811 7, 1989.

812 Bohn, T. J., Livneh, B., Oyster, J. W., Running, S. W., Nijssen, B. and Lettenmaier, D.
813 P.: Global evaluation of MTCLIM and related algorithms for forcing of
814 ecological and hydrological models. *Agric. For. Meteor.*, 176, 38–49,
815 <https://doi.org/10.1016/j.agrformet.2013.03.003>, 2013.

816 Boucher, M.-A., and Ramos, M.-H.: Ensemble Streamflow Forecasts for Hydropower
817 Systems. In *Handbook of Hydrometeorological Ensemble Forecasting*, edited by
818 Q. Duan, F. Pappenberger, J. Thielen, A. Wood, H.L. Cloke, and J.C. Schaake, 1–
819 19. Berlin Heidelberg: Springer, 2018.

820 Burn, D. H., and Boorman, D. B.: Estimation of hydrological parameters at ungauged
821 catchments. *J. Hydrol.*, 143,429454, <https://doi.org/10.1016/0022->
822 1694(93)90203-L, 1993.

823 Cai, X., Yang, Z.-L. , David, C. H., Niu, G.-Y. and Rodell, M.: Hydrological
824 evaluation of the Noah-MP land surface model for the Mississippi River Basin. *J.*
825 *Geophys. Res. Atmos.*, 119, 23–38, <https://doi.org/10.1002/2013JD020792>,
826 2014.

827 California Department of Water Resources: California data exchange center: Daily
828 full natural flow for December 2022. California Department of Water Resources,
829 accessed 1 October 2021, [https://cdec.water.ca.gov/reportapp/javareports?name=](https://cdec.water.ca.gov/reportapp/javareports?name=FNF)
830 FNF, 2021.

831 Cao, Q., Mehran, A. , Ralph, F. M. and Lettenmaier, D. P.: The role of hydrological
832 initial conditions on atmospheric river floods in the Russian River basin. *J.*
833 *Hydrometeor.*, 20, 16671686, <https://doi.org/10.1175/JHM-D-19-0030.1>, 2019.

834 Cao, Q., Gershunov, A., Shulgina, T., Ralph, F. M. , Sun, N. and Lettenmaier, D. P.:
835 Floods due to atmospheric rivers along the U.S. West Coast: The role of

836 antecedent soil moisture in a warming climate. *J. Hydrometeor.*, 21, 1827–1845,
837 [https:// doi.org/10.1175/JHM-D-19-0242.1](https://doi.org/10.1175/JHM-D-19-0242.1), 2020.

838 Castiglioni, S., Lombardi, L., Toth, E. , Castellarin, A. and Montanari, A.: Calibration
839 of rainfall-runoff models in ungauged basins: A regional maximum likelihood
840 approach. *Advances in Water Resources*, 33(10), 1235–1242.
841 <https://doi.org/10.1016/j.advwatres.2010.04.009>, 2010.

842 Chen, F., and Dudhia, J.: Coupling an advanced land surface–hydrology model with
843 the Penn State–NCAR MM5 modeling system. Part I: Model implementation
844 and sensitivity. *Mon. Wea. Rev.*, 129, 569–585, [https://doi.org/10.1175/1520-0493\(2001\)129<0569:CAALSH>2.0.CO;2](https://doi.org/10.1175/1520-0493(2001)129<0569:CAALSH>2.0.CO;2), 2001.

846 Chen, F., and Coauthors: Modeling of land-surface evaporation by four schemes and
847 comparison with FIFE observations. *J. Geophys. Res.*, 101, 7251–7268,
848 <https://doi.org/10.1029/95JD02165>, 1996.

849 Cosby, B.J., Hornberger, G.M., Clapp, R.B. and Ginn, T.: A statistical exploration of
850 the relationships of soil moisture characteristics to the physical properties of
851 soils. *Water resources research*, 20(6), 682-690, 1984.

852 [Demaria, E. M., Nijssen, B., & Wagener, T.: Monte Carlo sensitivity analysis of land](#)
853 [surface parameters using the Variable Infiltration Capacity model. *Journal of*](#)
854 [Geophysical Research](#), 112, D11113. <https://doi.org/10.1029/2006JD007534>,
855 [2007.](#)

856 [Demirel, M. C., Mai, J., Mendiguren, G., Koch, J., Samaniego, L., and Stisen, S.:](#)
857 [Combining satellite data and appropriate objective functions for improved spatial](#)
858 [pattern performance of a distributed hydrologic model, *Hydrol. Earth Syst. Sci.*,](#)
859 [22, 1299–1315, <https://doi.org/10.5194/hess-22-1299-2018>, 2018.](#)

860 Dickinson, R. E., Henderson-Sellers, A. & Kennedy, P. J.: Biosphere–Atmosphere
861 Transfer Scheme (BATS) version 1e as coupled to the NCAR Community

862 Climate Model. NCAR Tech. Note TN383+STR, NCAR, 1993.

863 Duan, Q., Sorooshian, S. and Gupta, V. : Effective and efficient global optimization
864 for conceptual rainfall-runoff models. Water Resour. Res., 28, 1015–1031,
865 [https://doi.org/ 10.1029/91WR02985](https://doi.org/10.1029/91WR02985), 1992.

866 Environmental Protection Agency (EPA) Office of Water: Low Flow Statistics Tools:
867 A How-To Handbook for NPDES Permit Writers. EPA-833-B-18-001, 2018.

868 Falcone, J.: GAGES-II: Geospatial attributes of gages for evaluating streamflow. U.S.
869 Geological Survey, accessed 1 April 2021,
870 [https://water.usgs.gov/GIS/metadata/usgswrd/XML/ gagesII_Sept2011.xml](https://water.usgs.gov/GIS/metadata/usgswrd/XML/gagesII_Sept2011.xml),
871 2011.

872 Federal Institute of Hydrology: “SOSRHINE.”
873 http://sosrhine.euporias.eu/en/sosrhine_overview, 2020.

874 Fisher, R.A. and Koven, C.D.: Perspectives on the future of land surface models and
875 the challenges of representing complex terrestrial systems. Journal of Advances
876 in Modeling Earth Systems, 12(4), p.e2018MS001453, 2020.

877 [Franchini, M., Galeati, G. and Berra S.: Global optimization techniques for the](#)
878 [calibration of conceptual rainfall-runoff models, Hydrol. Sci. J., 43, 443 – 458,](#)
879 [1998.](#)

880 [Gao, H., Birkel, C., Hrachowitz, M., Tetzlaff, D., Soulsby, C., & Savenije, H. H.](#)
881 [\(2018\). A simple topography-driven, calibration-free runoff generation model.](#)
882 [Hydrology and earth system sciences discussions.,1–42.](#)
883 <https://doi.org/10.5194/hess-2018-141>

884 Gochis, D. and Coauthors: Overview of National Water Model Calibration: General
885 strategy and optimization. National Center for Atmospheric Research, accessed 1
886 January 2023, 30 pp.,
887 https://ral.ucar.edu/sites/default/files/public/9_RafieeiNasab_CalibOverview_CU

888 AHSI_Fall019_0.pdf, 2019.

889 Gong, W., Duan, Q., Li, J., Wang, C., Di, Z., Dai, Y., et al.: Multi-objective parameter
890 optimization of common land model using adaptive surrogate modeling.
891 Hydrology and Earth System Sciences, 19(5), 2409–2425.
892 <https://doi.org/10.5194/hess-19-2409-2015>, 2015.

893 Gou, J., Miao, C., Duan, Q., Tang, Q., Di, Z., Liao, W., Wu, J. and Zhou, R.:
894 Sensitivity analysis-based automatic parameter calibration of the VIC model for
895 streamflow simulations over China. Water Resources Research, 56(1),
896 e2019WR025968, 2020.

897 Gupta, H. V., et al.: Decomposition of the mean squared error and NSE performance
898 criteria: Implications for improving hydrological modelling. Journal of
899 Hydrology, 377, 80-91,2009.

900 Holtzman, N.M., Pavelsky, T.M., Cohen, J.S., Wrzesien, M.L. and Herman, J.D.:
901 Tailoring WRF and Noah-MP to improve process representation of Sierra
902 Nevada runoff: Diagnostic evaluation and applications. Journal of Advances in
903 Modeling Earth Systems, 12(3), p.e2019MS001832, , 2020.

904 Hussein, A.: Process-based calibration of WRF-hydro model in unregulated
905 mountainous basin in Central Arizona. M.S. thesis, Ira A. Fulton Schools of
906 Engineering, Arizona State University, 110 pp.,
907 [https://keep.lib.asu.edu/_flysystem/fedora/
908 c7/224690/Hussein_asu_0010N_19985.pdf](https://keep.lib.asu.edu/_flysystem/fedora/c7/224690/Hussein_asu_0010N_19985.pdf), 2020.

909 [Imhoff, R.O., Van Verseveld, W.J., Van Osnabrugge, B. and Weerts, A.H.: Scaling
910 point-scale \(pedo\) transfer functions to seamless large-domain parameter
911 estimates for high-resolution distributed hydrologic modeling: An example for
912 the Rhine River. Water Resources Research, 56\(4\), p.e2019WR026807,2020.](#)

913 Kimball, J. S., Running, S. W. and Nemani, R. R.: An improved method for

914 estimating surface humidity from daily minimum temperature. *Agric. For.*
915 *Meteor.*, 85, 87–98, [https://doi.org/10.1016/S0168-1923\(96\)02366-0](https://doi.org/10.1016/S0168-1923(96)02366-0), 1997.

916 Lahmers, T.M., et al.: Evaluation of NOAA national water model parameter
917 calibration in semiarid environments prone to channel infiltration. *Journal of*
918 *Hydrometeorology*, 22(11), 2939-2969, 2021.

919 Li, D., Lettenmaier, D. P., Margulis, S. A. and Andreadis, K.: The role of rain-on-
920 snow in flooding over the conterminous United States. *Water Resour. Res.*, 55,
921 8492–8513, <https://doi.org/10.1029/2019WR024950>, 2019.

922 Liang, X., Lettenmaier, D. P., Wood, E. F. and Burges S. J. : A simple hydrologically
923 based model of land surface water and energy fluxes for general circulation
924 models, *J. Geophys. Res.*, 99(D7), 14415–14428, doi:10.1029/94JD00483, 1994.

925 Livneh B, Rosenberg, E.A., Lin, C., Nijssen, B., Mishra, V., Andreadis, K.,
926 Maurer, E.P. and Lettenmaier, D.P.: A long-term hydrologically based data set of
927 land surface fluxes and states for the conterminous United States: Updates and
928 extensions, *Journal of Climate*, doi:10.1175/JCLI-D-12-00508.1, 2013.

929 Maidment, D.R.: Conceptual Framework for the National Flood Interoperability
930 Experiment. *Journal of the American Water Resources Association* 53: 245–57,
931 2017.

932 Mascaro, G., Hussein, A., Dugger, A. and Gochis, D.J.: Process-based calibration of
933 WRF-Hydro in a mountainous basin in southwestern US. *Journal of the*
934 *American Water Resources Association*, 59(1), 49-70, 2023.

935 Mendoza, P.A., Clark, M.P., Mizukami, N., Newman, A.J., Barlage, M., Gutmann,
936 E.D., Rasmussen, R.M., Rajagopalan, B., Brekke, L.D. and Arnold, J.R.: Effects
937 of hydrologic model choice and calibration on the portrayal of climate change
938 impacts. *Journal of Hydrometeorology*, 16(2), 762-780, 2015.

939 Miller, D.A. and White, R.A.: A conterminous United States multilayer soil

940 characteristics dataset for regional climate and hydrology modeling. Earth
941 interactions, 2(2), pp.1-26, 1998.

942 [Mizukami, N., Clark, M. P., Newman, A. J., Wood, A. W., Gutmann, E. D., Nijssen,
943 B. , Rakovec, O. and Samaniego, L. :Towards seamless large-domain parameter
944 estimation for hydrologic models. Water Resour. Res., 53, 8020–8040. \[https://
945 doi.org/10.1002/2017WR020401\]\(https://doi.org/10.1002/2017WR020401\), 2017.](#)

946 Naeini, M.R., Analui, B., Gupta, H.V., Duan, Q. and Sorooshian, S.. Three decades of
947 the Shuffled Complex Evolution (SCE-UA) optimization algorithm: Review and
948 applications. Scientia Iranica, 26(4), pp.2015-2031, 2019.

949 [Natural Resources Conservation Service: SNOTEL \(Snow Telemetry\) Data. USDA.
950 <https://www.nrcs.usda.gov/wps/portal/wcc/home/>, 2023.](#)

951 Niu, G.-Y., Yang, Z.-L. , Dickinson, R. E. , Gulden, L. E. and Su, H.: Development of
952 a simple groundwater model for use in climate models and evaluation with
953 gravity recovery and climate experiment data. J. Geophys. Res., 112, D07103,
954 <https://doi.org/10.1029/2006JD007522>. 2007.

955 Niu, G. Y., Yang, Z. L., Dickinson, R. E., & Gulden, L. E.: A simple TOPMODEL-
956 based runoff parameterization (SIMTOP) for use in global climate models.
957 Journal of Geophysical Research: Atmospheres, 110(D21), 2005.

958 Niu, G.-Y., and Coauthors: The community Noah land surface model with
959 multiparameterization options (Noah-MP): 1. Model description and evaluation
960 with local-scale measurements. J. Geophys. Res., 116, D12109,
961 <https://doi.org/10.1029/2010JD015139>, 2011.

962 NOAA (National Oceanic and Atmospheric Administration): National Water Model:
963 Improving NOAA's Water Prediction Services, 2016.

964 Oubeidillah, A. A., Kao, S.-C., Ashfaq, M. , Naz, B. S. and Tootle, G.: A large-scale,
965 high-resolution hydrological model parameter data set for climate change impact

966 assessment for the conterminous US. Hydrology and Earth System Sciences,
967 18(1), 67–84. <https://doi.org/10.5194/hess-18-67-2014>, 2014.

968 Prata, A.J.: A new long-wave formula for estimating downward clear-sky radiation at
969 the surface. Quarterly Journal of the Royal Meteorological Society, 122(533),
970 1127-1151, 1996.

971 Poissant, D., Arsenault, A. and Brissette, F. : Impact of parameter set dimensionality
972 and calibration procedures on streamflow prediction at ungauged catchments. J.
973 Hydrol. Reg. Stud., 12,220–237, <https://doi.org/10.1016/j.ejrh.2017.05.005>,
974 2017.

975 Qi, W.Y., Chen, J. , Li, L. , Xu, C.-Y. , Xiang, Y.-h. , Zhang, S.-B. and Wang, H.-M.:
976 Impact of the number of donor catchments and the efficiency threshold on
977 regionalization performance of hydrological models. J. Hydrol., 601, 126680,
978 <https://doi.org/10.1016/j.jhydrol.2021.126680>, 2021.

979 Raff, D., Brekke, L. , Werner, K. , Wood, A. and White. K.: Short-Term Water
980 Management Decisions: User Needs for Improved Climate, Weather, and
981 Hydrologic Information. U.S. Bureau of Reclamation.
982 <https://www.usbr.gov/research/st/roadmaps/WaterSupply.pdf>, 2013.

983 Razavi, T., and Coulibaly, P.: An evaluation of regionalization and watershed
984 classification schemes for continuous daily streamflow prediction in ungauged
985 watersheds. Can. Water Resour. J., 42,2–20,
986 <https://doi.org/10.1080/07011784.2016.1184590>, 2017.

987 [Rajsekhar, D., Singh, V.P. and Mishra, A.K., 2015. Hydrologic drought atlas for](#)
988 [Texas. Journal of Hydrologic Engineering, 20\(7\), p.05014023.](#)

989 Schaake, J. C., Koren, V. I., Duan, Q.-Y., Mitchell, K., & Chen, F.: Simple water
990 balance model for estimating runoff at different spatial and temporal scales.
991 Journal of Geophysical Research, 101(D3), 7461–7475.

992 <https://doi.org/10.1029/95JD02892>, 1996.

993 Schaperow J.R, Li, D., Margulis, S.A., Lettenmaier D.P. :A near-global, high
994 resolution land surface parameter dataset for the variable infiltration capacity
995 model. Scientific Data. Aug 11;8(1):216, 2021.

996 [Schweppe, R., Thober, S., Müller, S., Kelbling, M., Kumar, R., Attinger, S., and](#)
997 [Samaniego, L.: MPR 1.0: a stand-alone multiscale parameter regionalization tool](#)
998 [for improved parameter estimation of land surface models, Geosci. Model Dev.,](#)
999 [15, 859–882, https://doi.org/10.5194/gmd-15-859-2022, 2022.](#)

1000 Sharma, P. and Machiwal, D.: Streamflow forecasting: overview of advances in data-
1001 driven techniques. Advances in Streamflow Forecasting,1-50.

1002 <https://doi.org/10.1016/B978-0-12-820673-7.00013-5>, 2021

1003 Shi, X., Wood, A.W. and Lettenmaier, D.P. : How essential is hydrologic model
1004 calibration to seasonal streamflow forecasting? Journal of Hydrometeorology,
1005 9(6), 1350-1363, 2008.

1006 Sofokleous, I., Bruggeman, A., Camera, C. and Eliades, M.: Grid-based calibration of
1007 the WRF-Hydro with Noah-MP model with improved groundwater and
1008 transpiration process equations. Journal of Hydrology, 617, 128991 , 2023

1009 Su, L., Cao, Q. , Xiao, M., Mocko, D. M., Barlage, M. , Li, D. , Peters-Lidard, C. D.
1010 and Lettenmaier, D. P.: Drought variability over the conterminous United States
1011 for the past century. J. Hydrometeor., 22, 1153–1168,
1012 <https://doi.org/10.1175/JHM-D-20-0158.1>, 2021.

1013 Su, L., Cao, Q. , Shukla, S., Pan, M. and Lettenmaier, D.P.: Evaluation of Subseasonal
1014 Drought Forecast Skill over the Coastal Western United States. Journal of
1015 Hydrometeorology, 24(4), 709-726, 2023.

1016 Tangdamrongsub, N.: Comparative Analysis of Global Terrestrial Water Storage
1017 Simulations: Assessing CABLE, Noah-MP, PCR-GLOBWB, and GLDAS

1018 Performances during the GRACE and GRACE-FO Era. *Water*, 15(13), p.2456,
1019 2023.

1020
1021 Thornton, P. E., and Running, S. W.: An improved algorithm for estimating incident
1022 daily solar radiation from measurements of temperature, humidity, and
1023 precipitation. *Agric. For. Meteor.*, 93, 211–228, [https://doi.org/10.1016/S0168-](https://doi.org/10.1016/S0168-1923(98)00126-9)
1024 1923(98) 00126-9, 1999.

1025 Tolson, B. A., and Shoemaker, C. A.: Dynamically dimensioned search algorithm for
1026 computationally efficient watershed model calibration. *Water Resour. Res.*, 43,
1027 W01413, <https://doi.org/10.1029/2005WR004723>, 2007.

1028 Troy, T. J., Wood, E. F. and Sheffield, J.: An efficient calibration method for
1029 continental-scale land surface modeling. *Water Resources Research*, 44,
1030 W09411. <https://doi.org/10.1029/2007WR006513>, 2008

1031 USWRC: Guidelines for determining flood flow frequency. Bulletin 17B of the
1032 Hydrology Subcommittee, 183 pp., [https://](https://water.usgs.gov/osw/bulletin17b/dl_flow.pdf)
1033 water.usgs.gov/osw/bulletin17b/dl_flow.pdf, 1982.

1034 Yang, Y., Pan, M., Beck, H.E. , Fisher, C.K., Beighley, R.E. , Kao, S.C. , Hong, Y. and
1035 Wood, E.F.: In quest of calibration density and consistency in hydrologic
1036 modeling: Distributed parameter calibration against streamflow characteristics.
1037 *Water Resources Research*, 55(9), 7784-7803, 2019.

1038 ~~Yang, Z. L., and Dickinson R. E. : Description of the BiosphereAtmosphere Transfer~~
1039 ~~Scheme (BATS) for the soil moisture workshop and evaluation of its~~
1040 ~~performance, *Global Planet. Change*, 13, 117–134, doi:10.1016/0921-~~
1041 ~~8181(95)00041-0, 1996.~~

1042 Yadav, M., Wagener, T., & Gupta, H. (2007). Regionalization of constraints on
1043 [expected watershed response behavior for improved predictions in ungauged](#)

Formatted: No underline, Font color: Auto

1044 [basins. *Advances in Water Resources*, 30\(8\), 1756–1774.](#)
1045 <https://doi.org/10.1016/j.advwatres.2007.01.005>
1046 Zheng, H., Yang, Z.-L. , Lin, P. , Wei, J. , Wu, W.-Y., Li, L. , Zhao, L. and Wang, S.:
1047 On the sensitivity of the precipitation partitioning into evapotranspiration and
1048 runoff in land surface parameterizations. *Water Resour. Res.*, 55, 95–111,
1049 <https://doi.org/10.1029/2017WR022236>, 2019.
1050 [Zink M, Mai J, Cuntz M, Samaniego L. Conditioning a hydrologic model using](#)
1051 [patterns of remotely sensed land surface temperature. *Water Resources Research*.](#)
1052 [2018 Apr;54\(4\):2976-98.](#)
1053